Available online at www.sciencedirect.com
SCIENCE DIRECT®
Journal of Power Sources 154 (2006) 518–522
JOURNAL OF POWER SOURCES
www.elsevier.com/locate/jpowsour

Short communication

Current distribution over the electrode surface in a cylindrical VRLA cell during discharge

Petr Křivák [a], Petr Bača [a], Milan Calábek [a], Karel Micka [b,*], Petr Král [a]

[a] *Department of Electrotechnology, Technical University, 602 00 Brno, Czech Republic*
[b] *J. Heyrovský Institute of Physical Chemistry, 182 23 Prague 8, Czech Republic*

Available online 28 November 2005

Abstract

The current distribution over the surface of cylindrical VRLA accumulator electrodes for hybrid electric vehicles during discharge was determined mathematically by using an equivalent electrical circuit. The dependence of the internal resistance on the current and on the charge passed was determined by measurements on an experimental cell. The results are presented in the form of 3D diagrams for different states of discharge. The effect of the configuration of the current tabs on the current distribution over the electrode surface during discharge is discussed.

Keywords: Grid design; Current distribution; Cylindrical lead-acid cell

1. Introduction

Valve-regulated lead-acid cells of cylindrical type are being developed for use in hybrid electric vehicles since they can combine the best attributes of the high-power VRLA designs (low resistance and high compression) with a more efficient thermal management; very good results were obtained with 12 V VRLA spiral wound batteries under power assist profile [1]. Since we have shown in our preceding theoretical work [2] that the configuration of current tabs may play a considerable role in utilization of the active material of plate accumulator electrodes during discharge with elevated currents, it seemed worth while to examine also the spiral wound cell electrodes from this point of view. The results of this study form the subject of our present work.

2. Equivalent circuit and input data

It is assumed that the positive and negative grids have equal numbers of meshes of equal forms, thus corresponding, in the geometrical sense, to each other (Fig. 1). Essentially, the mathematical model is based on an electrical equivalent circuit analogous to that used in our preceding work [2]. Part of this circuit corresponding to an elementary cell is shown in Fig. 2. The nodes are visualized by black points. The effective ohmic resistances of the horizontal and vertical half grid members including active mass are denoted as R_x and R_y, respectively, with superscript (+ or −) referring to the plate sign. The elementary resistances of the positive and negative grids were determined as follows:

$$R_x^+ = 4.33 \times 10^{-3}\,\Omega \qquad R_y^+ = 1.732 \times 10^{-3}\,\Omega$$
$$R_x^- = 3.215 \times 10^{-3}\,\Omega \qquad R_y^- = 9.285 \times 10^{-4}\Omega$$
$$R_{xo} = 4.48 \times 10^{-4}\,\Omega \tag{1}$$

where R_x denotes the resistance of a horizontal rib section of 4 mm in length, R_y the resistance of a vertical rib section, 10 mm in length, and R_{xo} resistance of a frame section of 4 mm in length.

The internal resistance of an elementary cell is denoted as Rv with a whole-numbered subscript (k). Similarly, the node potentials are denoted as V_k or W_k The internal resistances, Rv_k (in Ω), between the cell elements depend on the local discharge current, I_k (in amperes), and on the charge passed, Q_k (in C), corresponding to the kth node. The course of this functional dependence was determined on a laboratory cell for various discharge currents as in our preceding communication [2]. The values of Rv_k involving the electrolyte resistance, contact resistance between the lead grid and the active mass, the active mass resistance, and the polarization resistance were fitted by the following exponential function by using the least squares method:

$$Rv_k = 3.18 + 23000 \times Q_k I_k + 1.5 \times 10^{-11} \times \exp(4565 Q_k + 2556 I_k - 28) \tag{2}$$

* Corresponding author.
E-mail address: micka@jh-inst.cas.cz (K. Micka).

0378-7753/$ – see front matter © 2005 Elsevier B.V. All rights reserved.
doi:10.1016/j.jpowsour.2005.10.029

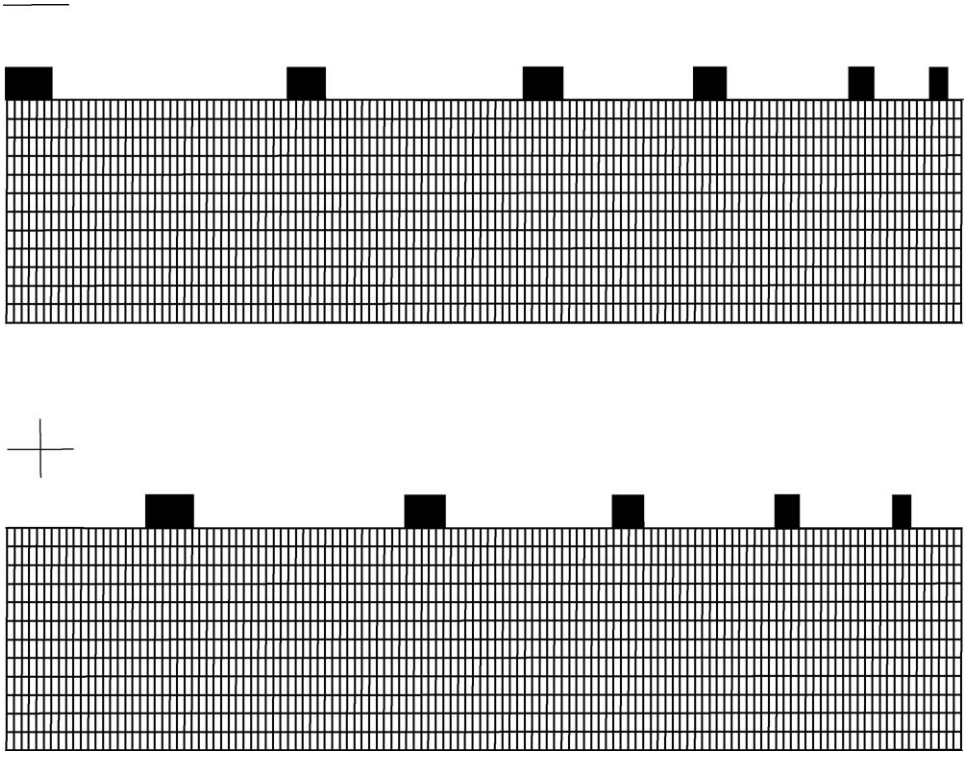

Fig. 1. Unrolled cylindrical cell electrode grids (top: negative, bottom: positive). Grid length 516 mm, height 120 mm.

The smoothed dependence of Rv_k on Q_k at various discharge currents is shown in Fig. 3. It is apparent that the most significant increase of the resistance takes place when the end of discharge is approached. Also, as stated previously [2], the resistance increase occurs earlier at higher currents.

With the positive electrode, the contribution of the active mass to the conductivity of the grid is only slight. However, with the negative electrode, the contribution of the active mass to the grid conductivity is considerable, and therefore, it must be taken into account in the calculations. It has been found that the conductance of the negative active mass decreases during the discharge approximately linearly with the charge passed [3]. By analogous considerations as in our preceding work [2], the dependence of the elementary resistances of the negative electrode on the charge

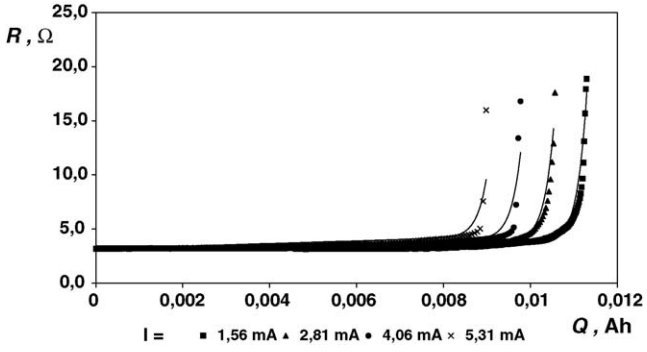

Fig. 3. Dependence of internal resistance of an electrode element (a grid mesh) on the charge passed at discharge currents varying from 1.56 to 5.31 mA. The experimental points were fitted by the model function (2).

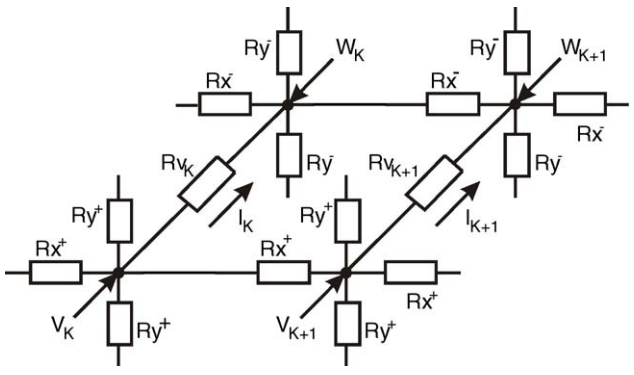

Fig. 2. Part of electrical equivalent circuit used to calculate the current distribution over the electrode surface.

passed may approximately be expressed as

$$R_x^- = \frac{1}{(310 - 4570Q_k)}, \qquad R_y^- = \frac{1}{(1077 - 28547Q_k)} \tag{3}$$

where $Q_k = \int I_k \mathrm{d}t$ and I_k is generally different for different nodes.

Thus, the electrode system can be build up by combining a number of three-dimensional meshes shown in Fig. 2.

3. Method of calculation

After application of the first and second Kirchhoff laws to nodes and loops of the whole equivalent circuit, a system of linear equations is obtained whose solution gives the sought

distribution of local potentials and currents. Since the resistances are time-dependent, the calculations were performed in the following steps:

Step 1: $i = 1$, $t_1 = 1$ s, $\Delta t_1 = 1$ s is set constant. All elements of the internal resistance, Rv_k, are set equal to their initial value of $R_1 = 3.18\ \Omega$ and the distribution of the potentials in the nodes of the equivalent circuit is calculated. The node potentials of the kth element, V_k^1 and W_k^1, are used to calculate the corresponding voltage and current:

$$U_k^1 = V_k^1 - W_k^1, \quad I_k^1 = \frac{U_k^1}{R_k^1} \tag{4}$$

The charge passed through the kth element is calculated from the current as

$$Q_k^1 = I_k^1 \times \Delta t_1 \tag{5}$$

Step 2: $i = 2$, $t_2 = 160$ s, $\Delta t_2 = t_2 - t_1$. The internal resistance corresponding to the k-th element is calculated from Eq. (2). Afterwards, the node potentials are calculated and from these, in turn, the corresponding values of voltage and currents are determined as in step 1. The charge passed through the kth element is then calculated as

$$Q_k^2 = Q_k^1 + I_k^2 \times \Delta t_2 \tag{6}$$

The calculations are continued according to step 2 up to the value of $t_n = 15{,}900$ s (100% state of discharge).

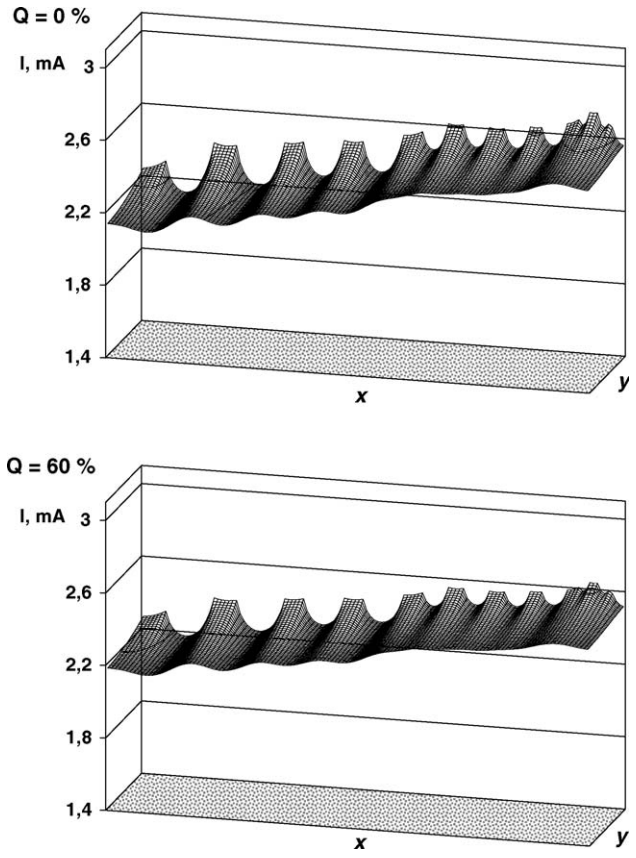

Figs. 4 and 5. Current distributions for an unrolled cylindrical cell at zero and 60% discharge.

The time step of $\Delta t = 159$ s is suitable since the errors due to linearization are negligible. Higher values of the time step cause higher linearization errors, and lower values lead to a sensible increase of the calculation time.

4. Results and discussion

The results of the calculation of the current distribution over the electrode surface are shown in the form of 3D diagrams in Figs. 4–8 for values of Q corresponding to 0, 60, 85, 95, and 100% discharge. The current values plotted correspond to an

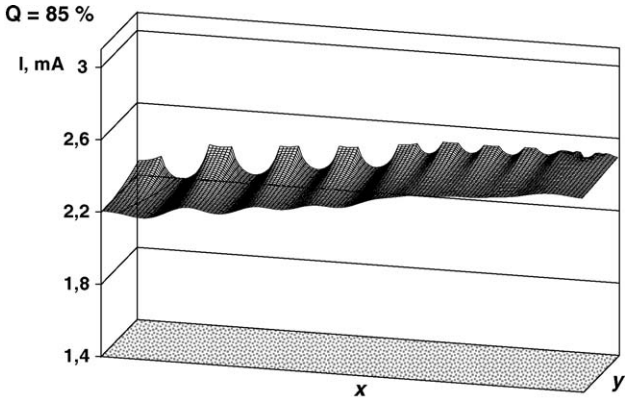

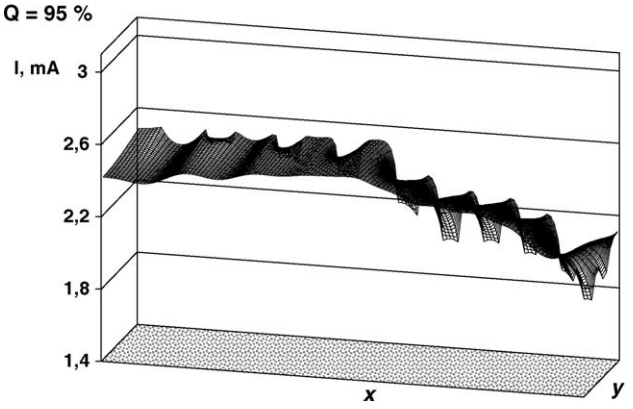

Figs. 6 and 7. Current distributions for an unrolled cylindrical cell at 85 and 95% discharge.

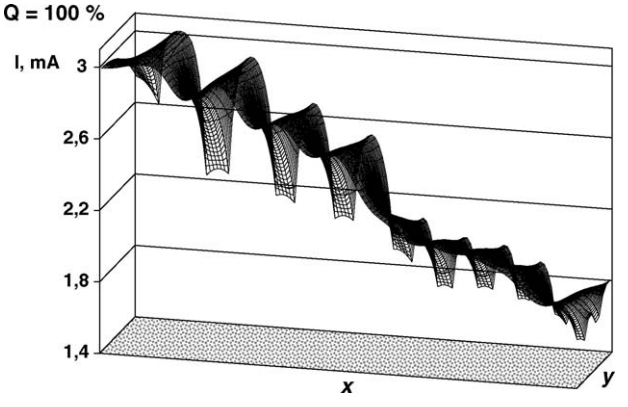

Fig. 8. Current distribution for an unrolled cylindrical cell at full discharge.

electrode element (cf. Eq. (4)). The total current was $I = 4$ A and the discharge capacity $C = 17.66$ Ah.

It is apparent from Figs. 4–8 that, at the beginning of discharge, the regions close to the current tabs are most appreciably loaded with the current, especially in the central region of the cylindrical cell where the tabs are closer to one another. (Note that the tabs of the positive grid are shifted against those of the negative.) Therefore, these regions are fully discharged first and so their internal resistance attains its highest value. Since the discharge current is kept constant, the decreasing current density in the regions of increasing internal resistance causes a current density increase in the other regions, especially in the last stage of discharge. This behaviour leads to gradual exploitation of all regions of the electrodes as the discharge continues, however, at the expense of increasing internal resistance. Nonuniformity of the current distribution in the cylindrical cell increases considerably close to the end of discharge.

For illustration, in Fig. 9 is shown a cross section of the resistance network for two cell variants differing by the configuration of the current tabs, with current leads close to one another at neighbouring electrode ends (A) and with current leads at opposite electrode ends (B). The current direction is denoted by arrows, R_c^+ and R_c^- denote the current lead resistances and the other symbols have the same meaning as in Fig. 2.

It is apparent from this figure that in case (A) the resistance in the current circuit increases with the distance from the current leads. This causes nonuniformity of the current distribution through the resistance network. At the beginning of discharge, the regions close to the current tabs are more loaded with the current than those lying apart. With continuing discharge, the internal resistance Rv_N close to the current tabs increases resulting in gradual increase of the discharge rate in the regions lying further apart.

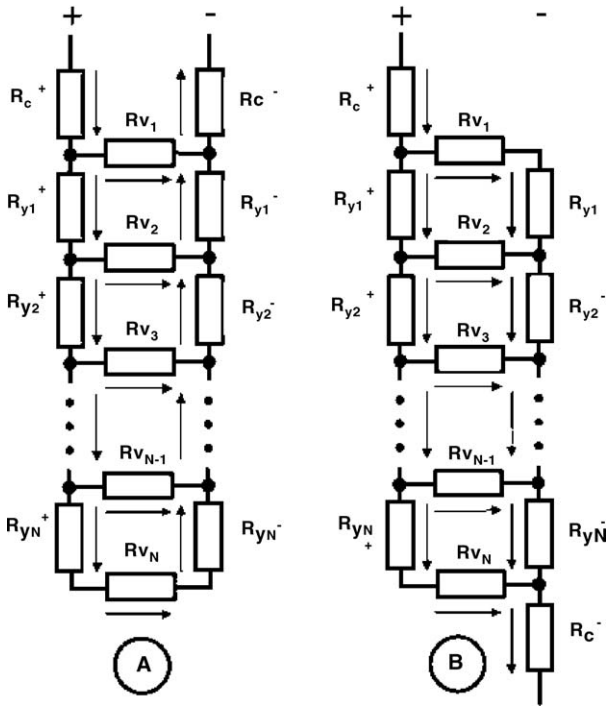

Fig. 9. Cross section of the cell resistance network for two cases: (A) current tabs located at the top of the electrodes, (B) current tabs located at opposite ends of the electrodes.

In case (B), thanks to the positioning of the current tabs (with the plausible assumption that the resistances of the vertical electrode elements, R_y^+ and R_y^-, are roughly equal) the current distribution over the electrode surface is practically uniform. This is substantiated by calculations of the current distribution for the case where extended current tabs are located at opposite ends of the electrodes (Fig. 10). In this case, the current distribu-

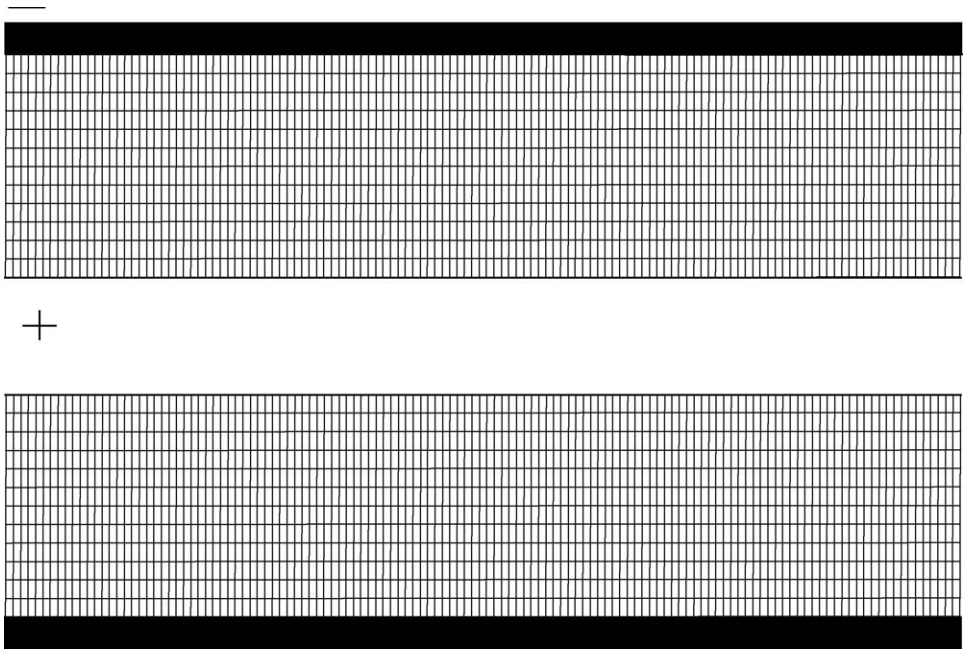

Fig. 10. Unrolled cylindrical cell electrode grids with extended tabs located at opposite ends of the electrodes (top: negative, bottom: positive). Same grid dimensions as in Fig. 1.

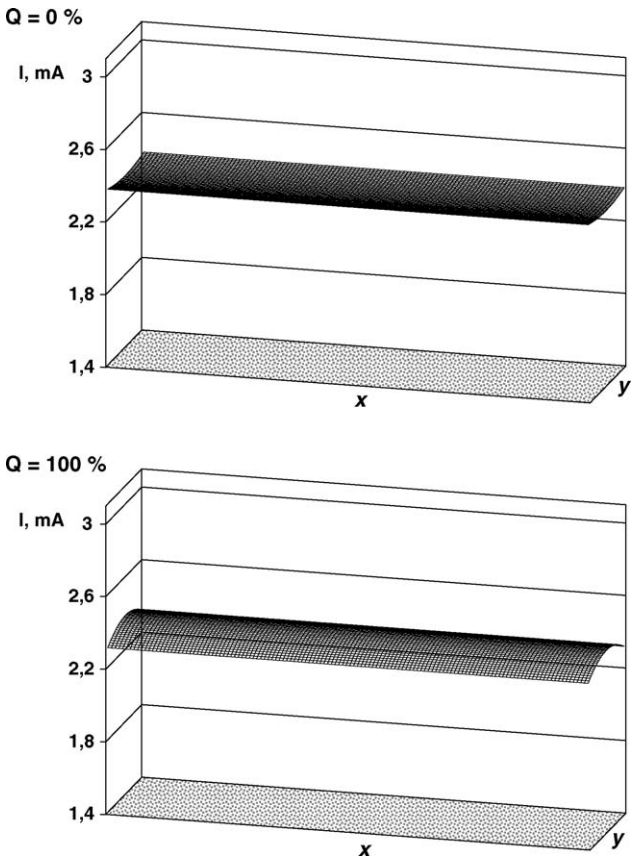

Figs. 11 and 12. Current distributions for an unrolled cylindrical cell with extended tabs located at opposite ends of the electrodes at zero and at full discharge.

tion during discharge is nearly uniform over the whole electrode area.

It may be of interest that the case of extended current tabs (Fig. 10) is amenable to a general analytical solution [3], since the mathematical problem is here only one-dimensional (only the y coordinate need be considered since the variables are independent of x). This solution allows prediction of the nonuniformity of the current distribution from the basic physical parameters of the lead-acid cell. The main result is that the nonuniformity increases with the plate electrode height and resistivities, whereas it decreases with the internal resistance, Rv. For the cell considered in the present work, the effect of the (rolled) electrode height is relatively small (Figs. 11 and 12).

5. Conclusion

It has been found that the current distribution over the electrode area is most uniform when the electrodes are provided with extended current tabs located at their opposite ends.

Acknowledgments

The authors are indebted to Dr. Francisco Trinidad, Tudor-Exide Technologies, Azuqueca de Henares (Guadalajara), Spain, for helpful interest and comments, and for kindly providing the original parts of the cylindrical cells. This work was supported by the Advanced Lead-Acid Battery Consortium (Project No. N4.2), a program of the International Lead Zinc Research Organization.

References

[1] F. Trinidad, C. Gimeno, J. Gutiérrez, R. Ruiz, J. Sainz, J. Valenciano, J. Power Sources 116 (2003) 128.
[2] P. Král, P. Křivák, P. Bača, M. Calábek, K. Micka, J. Power Sources 105 (2002) 35.
[3] M. Calábek, K. Micka, P. Bača, P. Křivák, J. Power Sources 85 (2000) 145.